Interannual variability in the atmospheric CO_2 rectification over a boreal forest region

Baozhang Chen and Jing M. Chen
Department of Geography and Program in Planning, University of Toronto, Toronto, Ontario, Canada

Douglas E. J. Worthy
Air Quality Research Branch, Meteorological Service of Canada, Toronto, Ontario, Canada

Received 25 October 2004; revised 12 April 2005; accepted 1 June 2005; published 19 August 2005.

[1] Ecosystem CO_2 exchange with the atmosphere and the planetary boundary layer (PBL) dynamics are correlated diurnally and seasonally. The strength of this kind of covariation is quantified as the rectifier effect, and it affects the vertical gradient of CO_2 and thus the global CO_2 distribution pattern. An 11-year (1990–1996, 1999–2002), continuous CO_2 record from Fraserdale, Ontario (49°52′29.9″N, 81°34′12.3″W), along with a coupled vertical diffusion scheme (VDS) and ecosystem model named Boreal Ecosystem Productivity Simulator (BEPS), are used to investigate the interannual variability of the rectifier effect over a boreal forest region. The coupled model performed well (r^2 = 0.70 and 0.87, at 40 m at hourly and daily time steps, respectively) in simulating CO_2 vertical diffusion processes. The simulated annual atmospheric rectifier effect varies from 3.99 to 5.52 ppm, while the diurnal rectifying effect accounted for about a quarter of the annual total (22.8∼28.9%).The atmospheric rectification of CO_2 is not simply influenced by terrestrial source and sink strengths, but by seasonal and diurnal variations in the land CO_2 flux and their interaction with PBL dynamics. Air temperature and moisture are found to be the dominant climatic factors controlling the rectifier effect. The annual rectifier effect is highly correlated with annual mean temperature (r^2 = 0.84), while annual mean air relative humidity can explain 51% of the interannual variation in rectification. Seasonal rectifier effect is also found to be more sensitive to climate variability than diurnal rectifier effect.

Citation: Chen, B., J. M. Chen, and D. E. J. Worthy (2005), Interannual variability in the atmospheric CO_2 rectification over a boreal forest region, *J. Geophys. Res.*, *110*, D16301, doi:10.1029/2004JD005546.

1. Introduction

[2] Over the past 3 decades, annual accumulation of CO_2 in the atmosphere varied significantly from year to year, ranging from about 1 GtC per year to as high as 6 GtC per year [*Conway et al.*, 1994] (data updates to Conway et al. are available from www.cmdl.noaa.gov/ccgg/). In recent years, the atmospheric CO_2 increase due to fossil fuel combustion has been around 2.8 PgC yr^{-1} (equivalent to 1.4 ppm yr^{-1}) [*Ishizawa et al.*, 2002; *Prentice et al.*, 2001; *Blasing et al.*, 2005] with a small year-to-year variability (<0.3 PgC yr^{-1}) [*Marland et al.*, 2002]. Therefore variations in the observational data primarily reflect variations in the ocean and land fluxes, with the global carbon sink ranging from about 1 GtC per year to perhaps as much as 5 GtC per year [*Keeling et al.*, 1995; *Francey et al.*, 1995]. To understand the response of global ecosystems to climate changes and anthropogenic perturbations and to predict future trends in atmospheric CO_2, it is critical to determine the spatial distribution of carbon sources and sinks and to understand the mechanisms for carbon sequestration [*Enting et al.*, 1995; *Enting*, 1999; *Wofsy and Harris*, 2002]. Unfortunately, spatial and temporal heterogeneities in the net exchange of CO_2 between the surface and the atmosphere make it impractical to derive regional or global values from direct measurements at small scales. Classic inversion (top-down) and ecosystem modeling (bottom-up) methods are both under-constrained for relevant spatial/temporal scales. An emerging question is whether it is possible to merge top-down and bottom-up approaches to use surface and atmospheric observations to constrain land-atmospheric exchanges at various spatial scales and at timescales of weeks, months, years and decades.

[3] Seasonal and diurnal covariance between net ecosystem CO_2 exchange (NEE) and the planetary boundary layer (PBL) dynamics, termed as the atmospheric rectification, influences the time-mean vertical partitioning of CO_2 between the PBL and the free troposphere (FT) [*Denning et al.*, 1995], and leads to significant spatial gradients in CO_2. The enhancement in the simulated annual mean Arctic-to-Antarctic CO_2 gradient in marine boundary layer (MBL) due to rectification, varies from slightly negative to more than 3 ppm among different transport models [*Law et al.*,

0148-0227/05/2004JD005546$09.00

1996; *Denning et al.*, 1999]. It is one of the largest sources of uncertainty in estimates of continental/global-scale carbon sinks/sources [*Gurney et al.*, 2002, 2003]. Understanding the rectification and quantifying its inter-annual variability as well as its influence on the distribution of CO_2 in the atmosphere is a key in being able combine top-down and bottom-up approaches. It also has the potential to significantly reduce uncertainties.

[4] Atmospheric inversion calculations infer the distribution of surface sources and sinks from time-averaged CO_2 distributions observed at remote marine boundary layer (MBL) locations [*Tans et al.*, 1990]. It is therefore not surprising that regional carbon sources/sinks derived from inverse model calculations are model-dependent, and especially sensitive to transport model representations of vertical mixing and horizontal advection [*Stephens et al.*, 2000]. Several recent studies have explored how the behavior of the PBL column integral CO_2 would help to reduce uncertainties associated with carbon sources and sinks in atmospheric inversions [*Olsen and Randerson*, 2004; *Rayner and O'Brien*, 2001]. For example, *Gloor et al.* [2000] showed that measurements of a single PBL column profile of CO_2 over the Amazon Basin would be one of the most effective ways, paradoxically, to reduce uncertainty associated with the size of the contemporary North American carbon sink. Similarly, *Rayner et al.* [2002] demonstrated that source/sink inversion results were found to be sensitive to biases caused by incomplete sampling of the diurnal cycle of the PBL column CO_2. These initial studies have also explored the applicability of using the PBL column integral CO_2 measurements to improving the estimation of the global/regional carbon sources/sinks in inverse calculation. The advantages of introducing the PBL column integral CO_2 into inverse modeling have been clearly shown in these studies. While diurnal, seasonal, and latitudinal aspects of CO_2 variability near the surface have been extensively explored [e.g., *Bolin and Keeling*, 1963; *Keeling et al.*, 1976; *Fung et al.*, 1987; *Wofsy et al.*, 1988; *Tans et al.*, 1990; *Bakwin et al.*, 1995; *Denning et al.*, 1996a; *Chou et al.*, 2002; *Gurney et al.*, 2002], unfortunately, very little is known about the behavior of the CO_2 column integral [*Olsen and Randerson*, 2004], Aircraft would have likely provided an adequate platform for such observations, particularly over continents [*Tans et al.*, 1996], however, high-frequency aircraft sampling is extremely expensive and does not provide continuous records. Observations on very tall towers can only reach the lower part of the convective planetary boundary (CBL) with the highest measurement level being around 500 m [*Bakwin et al.*, 1995, 1998a, 1998b]. The covariance between NEE and PBL dynamics drives the rectifier effect. Observations to constrain the strength of the rectification in nature are lacking [*Yi et al.*, 2004]. One way to retrieve this covariance information from tower CO_2 concentration measurements is to apply a model to simulate the temporal variation of CO_2 at given heights resulting from ecosystem metabolism and atmospheric diffusion in the PBL. The CO_2 data record collected over 11 years at Fraserdale from a 40 m high tower in a boreal forest region (Ontario, Canada; 49°52′, 81°37′W), is the longest continental record (1990–1996, 1999–present) within North America and as such provides an opportunity to study long-term and interannual variations of CO_2 behavior within the PBL as well as the interactions between the PBL and the FT. The hourly averaged CO_2 concentration record is used to test models for investigating the interannual variations in rectification and CO_2 sources and sinks in North America.

[5] Here we will explore two questions through investigating the interannual variability in the atmospheric rectifier effect: (1) How do the covariances among CO_2 net exchange, the mixing ratio and the PBL dynamics depend on daytime, nighttime, seasonal and annualCO_2 fluxes at the surface and (2) how do the differences between the PBL concentrations of CO_2 and the surface values observed at towers depend on these fluxes? Knowledge of these covariances and differences would provide a basis for us to use observations at individual towers to infer regional carbon cycle information at timescales of weeks, months, years and decades.

2. Materials and Methods

2.1. Research Site, Surrounding Landscape Characteristics, and Measurements

[6] The Fraserdale (FRD) tower is located southwest of James Bay in northern Ontario [*Higuchi et al.*, 2003]. The site is about 210 m above the sea level, with a 40-m tower located on the top of a small hill at the east end of a large clearing, about 300–400 m across, which is characterized by a relatively smooth shallow valley covered by tall grass and several small willow trees. According to a Landsat TM image at a 30 m resolution (1994), the landscape (3600 km^2 around the tower) consists of 66% of black spruce (*Picea mariana*) and Jack pine (*Pinus banksiana*), 20% open land after forest fires and logging, 11% aspen (*Populus tremuloides*) and paper birch (*Betula papyrifera*), and 3% open water.

[7] In February 1990, a continuous monitoring of atmospheric CO_2 was initiated at the 40-m tower at the FRD site. The second air sample intake was added at the 20 m in late 1995. The measurement continued until November 1996 with only a few short interruptions. Meteorological parameters, such as wind and air temperature, were measured at heights of 1.5,10, 20 and 40 m on the tower; humidity was taken at 1.5, 20 and 40 m levels. The measurement program was re-initiated in late 1998, and continues to the present-day. The measurements were made according to the WMO (Global Atmospheric Watch) guidelines, with an accuracy of 0.1 ppm [*Higuchi et al.*, 2003].

2.2. Modeling Methodology

2.2.1. Outline of the Model System

[8] The carbon cycle involving soil, vegetation and atmosphere and driven by solar and thermal energy is simulated using an integrated modeling system. This system consists of two components; the vertical diffusion scheme (VDS) [*Chen et al.*, 2004] and an ecosystem model, named "Boreal Ecosystem Productivity Simulator" (BEPS) [*Chen et al.*, 1999; *Liu et al.*, 1999, 2002]. VDS simulates CO_2 diffusion within the PBL under both stable and unstable conditions [*Chen et al.*, 2004]. The atmospheric stability determines the selection of a stable or free convection scheme. The criteria for the selection are the sign and

Table 1. Linear Regression Statistics Between Modeled and Observed CO_2 Mixing Ratio at the Surface Layer (40 m Height) for the Periods 1990–1996 and 1999–2002, Fraserdale, Ontario, Canada[a]

Timescale	MBE	RMSE	RMSD	r^2	N
hourly	1.08	5.76	1.57	0.70	87,980
10-day composite hourly	1.13	3.98	1.08	0.83	9383
daily	1.08	3.44	0.93	0.87	3666

[a]MBE is the mean bias error, $\sum_{i=1}^{N}\frac{C_{obs}(i)-C_{\mathrm{mod}}(i)}{N}$; RMSE is the root mean square error, $\sqrt{\frac{1}{N}\sum_{i=1}^{N}\left[C_{obs}(i)-C_{od}(i)\right]^2}$; RMSD is the root mean square difference expressed in percentage of the average of observed CO_2 mixing ratio, $\frac{RMSE}{\sum_{i=1}^{N}\frac{C_{obs}(i)}{N}}$; and r^2 is the squared linear regression coefficient,

$$\frac{N\sum_{i=1}^{N}(C_{obs}(i)C_{od}(i))-\sum_{i=1}^{N}C_{obs}(i)\sum_{i=1}^{N}C_{od}(i)}{\left(N\sum_{i=1}^{N}[C_{od}(i)]^2-\left[\sum_{i=1}^{N}C_{od}(i)\right]^2\right)\left(N\sum_{i=1}^{N}[C_{od}(i)]^2-\left[\sum_{i=1}^{N}C_{od}(i)\right]^2\right)}.$$

magnitude of the bulk Richardson number R_b in the surface layer and the magnitude of $|z_h/L|$, where z_h denotes the height of the mixed layer and L is the Monin-Obukhov length. R_b is calculated using equation (5.6.3) from *Stull* [1993]. BEPS and VDS are linked through three prognostic variables: land surface sensible heat flux (H) and latent heat flux affecting the mixed layer development, and net ecosystem carbon flux (NEE) driving vertical CO_2 transfer, which are calculated using BEPS at each computing time step.

2.2.2. Model Updates

[9] The BEPS model used in this study is an updated version (BEPS2.0) that includes a land surface scheme, named ''Ecosystem-Atmosphere Simulation Scheme'' (EASS), as a crucial component, in that energy, water and carbon cycles are fully coupled. EASS is similar to CLASS-C [*Arain et al.*, 2002; *Wang et al.*, 2002a, 2002b] and SiB2 [*Sellers et al.*, 1996, 1997], but is driven by remotely sensed surface parameters B. Chen et al., Remote sensing based ecosystem-atmosphere simulation Scheme (EASS)—Model formulation and test with multiple-year data, submitted to *Journal of Hydrometeorology*, 2005, and B. Chen et al., Modeling and scaling coupled energy, water, and carbon fluxes based on remote sensing: An application to Canada's landmass, submitted to *Journal of Hydrometeorology* 2005) (hereinafter referred to as Chen et al., submitted manuscript, 2005a and 2005b, respectively). This updated ecophysiology model simulates ecosystem processes including water balance, photosynthesis [*Farquhar et al.*, 1980], autotrophic and heterotrophic respiration, and radiation and energy balances of the canopy and soil surface. Preliminary experiments showed that the simulation realism and accuracy in carbon dynamics are enhanced significantly [*Ju et al.*, 2004].

[10] VDS has been updated since *Chen et al.* [2004]. A new module for simulating the stable boundary layer (SBL) is introduced in the new version. The diurnal evolution of SBL is not necessary for simulating CO_2 diffusion processes under stable atmospheric conditions according to the VDS modeling strategy. To simplify calculation, we only emphasize on simulating the equilibrium height of SBL, which is a baseline height for modeling CBL height. A diagnostic multilimit SBL height equation is introduced after *Zilitinkevich and Mironov* [1996], *Zilitinkevich and Baklanov* [2002], and *Zilitinkevich et al.* [2002],

$$h_E=\frac{C_n\mu_*}{|f_c|}\left[1+\frac{C_n^2\mu_*\left(1+C_{ir}NL/\mu_*\right)}{C_{sr}^2|f_c|L}\right]^{-1/2}, \qquad (1)$$

where C_n, C_{sr}, and C_{ir} are dimensionless constants, which are approximately set to 0.3, 1.0, and 1.7, respectively; f_c is the Coriolis parameter (= $2\omega \sin\phi$ = $(1.45 \times 10^{-4}\ s^{-1}) \times \sin|\phi|$, where ϕ is the latitude); μ_*, N, and L are the fraction velocity, the Brunt–Väisälä frequency, and the Monin–Obukhov length, respectively, which are calculated using the general equations cited from *Stull* [1993] (see Stull's equation (9.7.1b) for μ_*, equation (12.6.1a) for N, and equation (5.7c) for L).

[11] Moreover, the CBL module in VDS is modified by considering moisture buoyancy effects: (i) the potential temperature (θ) is replaced by the virtual potential temperature ($\theta_v = \theta + 0.61T_0q$, where T_0 is a reference value of absolute temperature, and q is the specific humidity); (ii) the flux of virtual potential temperature ($F_{\theta v}$) is introduced into VDS. We calculate $F_{\theta}v$ using equation (2) after *McNaughton and Spriggs* [1986],

$$F_{\theta v}=\frac{H+0.07\lambda E}{C_p\rho}, \qquad (2)$$

where H is the sensible heat flux (J m^{-2} s^{-1}), C_p is the heat capacity of air (= 29.2 J mol^{-1} K^{-1}), λ is the latent heat vaporization of water (= 43.7 × 103 J mol^{-1}), ρ is the air density in mol m^{-3}, and E is the surface evaporation rate (mol m^{-2} s^{-1}). H and E are simulated using the EASS model.

[12] The lower surface layer in VDS is set at a fixed height of 40 m. The model is improved through the use of shorter time steps and smaller spatial intervals (30 s versus 60 s and 50 m versus 100 m from *Chen et al.* [2004]).

2.2.3. Model Inputs

[13] The input data for this model system include the land surface parameters (i.e. vegetation and soil data) and meteorological variables measured over the canopy height. The

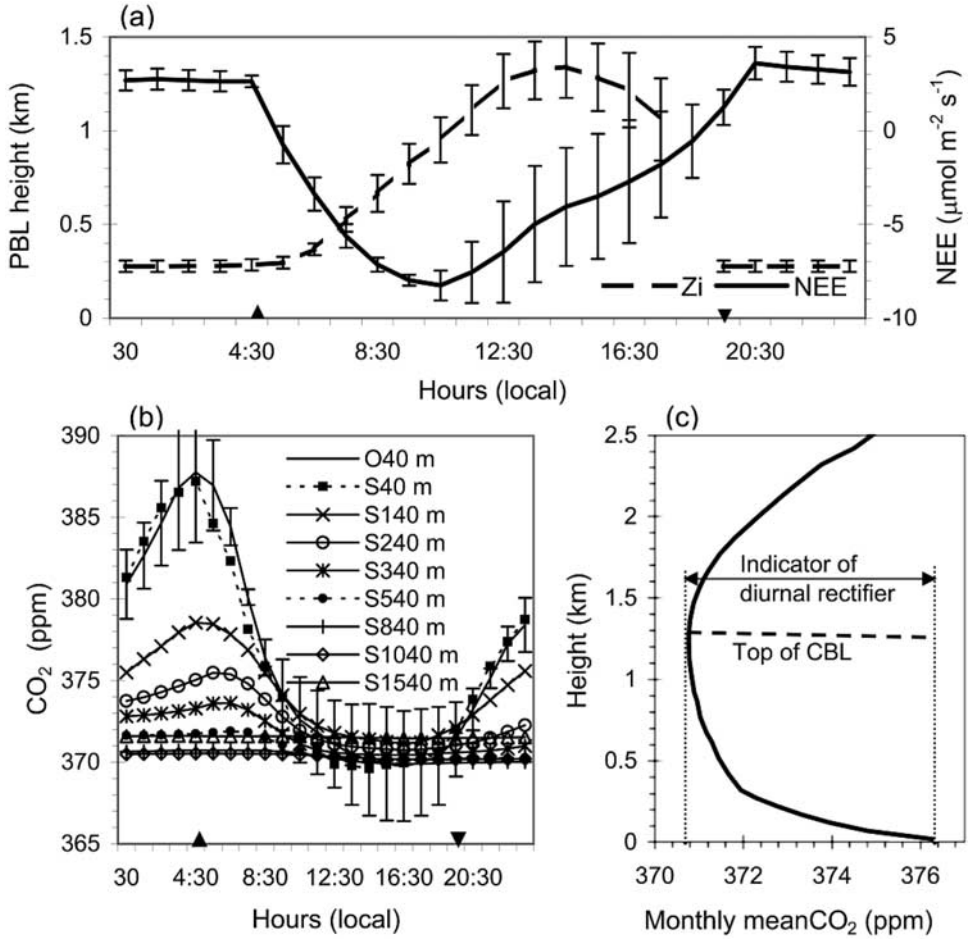

Figure 1. Schematic showing the diurnal rectification mechanism. An example from tower observations and simulations for June 2002, over a boreal region near Fraserdale, Ontario, Canada. (a) Simulated monthly composite diurnal dynamics of the planetary boundary layer (Z_i, thick dashed line) and the net ecosystem CO_2 exchange (NEE, thick solid line), the bars indicate standard deviation; (b) observed (O40 m: at 40 m height, solid line with standard error bars) and simulated monthly averaged diurnal cycles of CO_2 at various heights (S40∼S1540 m, without error bars); and (c) a simulated vertical profile of monthly mean CO_2. Triangles indicate the times of sunrise and sunset.

vegetation parameters (i.e., land cover type and leaf area index) are derived from satellite images at 1-km resolution (directly from AVHRR images, or up-scaling from Landsat TM) instead of directly using observed canopy data. Data on total soil dead organic matter (DOM) and soil texture are obtained from the Soil Landscapes of Canada (SLC) database, the best soil database currently available for the country [*Shields et al.*, 1991; *Schut et al.*, 1994, *Tarnocai*, 1996; *Lacelle*, 1998]. The soil textural data (silt and clay fraction) and DOM data at the FRD site are extracted from the map of SLC version 2.0.

[14] The hourly meteorological data as model inputs include air temperature, air relative humidity, incoming shortwave radiation, wind speed, precipitation, and air pressure. Unfortunately, for the FRD tower, precipitation is not measured and incoming shortwave radiation is not available for the period 1990–1996. We approximately use the precipitation data measured at the weather station Kapuskasing (87 km southwest of FRD) as a proxy. In order to estimate solar irradiance when the data are not available, a solar irradiance module is used after the modified Bristow-Campbell algorithms. The total daily solar irradiance (R_s) is calculated from the limited data set of daily maximum and minimum air temperature and daily total precipitation, along with site latitude, elevation, and annual mean temperature [*Bristow and Campbell*, 1984; *Winslow et al.*, 2001] (see Appendix A for more details).

[15] Moreover, the Globalview reference MBL matrix data are used as model top boundary condition instead of CBA flask station data used by *Chen et al.* [2004]. The matrix data from NOAA/CMDL's network is constructed in weekly intervals with spatial increment of 0.05 sine of latitude on the basis of sampling sites located in the marine boundary layer [*GLOBALVIEW-CO2*, 2004]. We use a linear interpolation method to extract MBL matrix values of CO_2 mixing ratio for the FRD site.

2.2.4. Model Validation

[16] BEPS has been validated for several sites (campaign data or eddy covariance measurements) over Canada [*Liu et al.*, 1997, 1999, 2002; *Ju et al.*, 2004]. It has also been applied to other ecosystems with acceptable

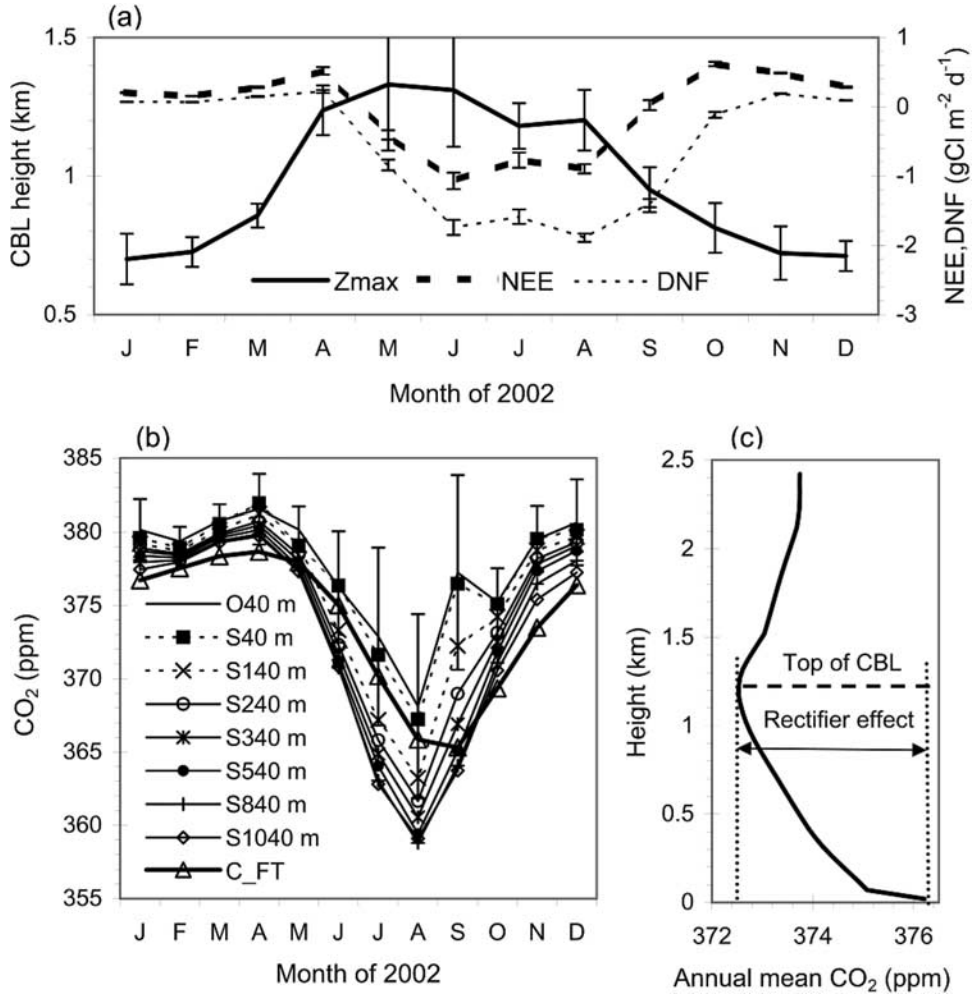

Figure 2. Schematic showing the seasonal rectification mechanism. An example from tower observations and simulations for 2002, over a boreal region near Fraserdale, Ontario, Canada. (a) Monthly averages of convective boundary layer depth (Z_{max}), net ecosystem CO_2 exchange (NEE) and daytime net CO_2 flux (DNF), the bars indicate the standard deviation; (b) observed (O40 m: at 40 m height, solid line with standard error bars) and simulated monthly mean CO_2 concentrations at different heights (S40∼S1540 m, without error bars); the background values, monthly mean CO_2 concentration in the free troposphere (the interpolated CO_2 mixing ratio for the latitudes where FRD site is located from Globalview reference MBL matrix data, thick solid line with triangles), were also shown here for a comparison; and (c) a simulated vertical profile of annual mean CO_2.

results [*Sun et al.*, 2004, *Wang et al.*, 2003; *Matsushita et al.*, 2002, 2004]. EASS has been tested and validated against multiple-year observed data at several sites over Canada. Overall, EASS is proved to be successful in capturing variations in energy fluxes, canopy and soil temperatures, and soil moisture over diurnal, synoptic, seasonal and inter-annual temporal scales (Chen et al., submitted manuscript, 2005a, 2005b).

[17] The integrated VDS model system is validated against hourly averaged CO_2 concentrations at 40 m height for the 11-year record. The results are summarized in Table 1 in term of regression statistics between modeled and observed CO_2 concentrations at different timescales. The values of squared linear regression coefficients (r^2) increase, and the root mean square errors (RMSE) and the mean bias errors (MBE) decrease as the modeled hourly values are averaged for daily and 10-day composite diurnal cycles, suggesting that the 1-d model can capture the underlying ecosystem variability for regional carbon balance estimation. The root mean square differences (RMSD) (percentage of the averaged observations), are lower than 2% across different timescales. This suggests that VDS has capacity of capturing most variations in CO_2 mixing ratios at the surface layer. Simulated vertical patterns of CO_2 mixing ratios are also comparable with those measured at the North Carolina tower [*Chen et al.*, 2004]. To further verify model performance in simulating vertical diffusion processes, VDS has recently been applied to the WLEF tower [*Chen et al.*, 2005]. VDS is validated against observed CO_2 mixing ratios at the heights of 30 m, 122 m, and 396 m for 2001. The regression statistics show that the values of r^2 at hourly time steps equal 0.69, 0.79 and 0.83 for 30 m, 122 m and 396 m, respectively. Correspondingly, the RMSE values

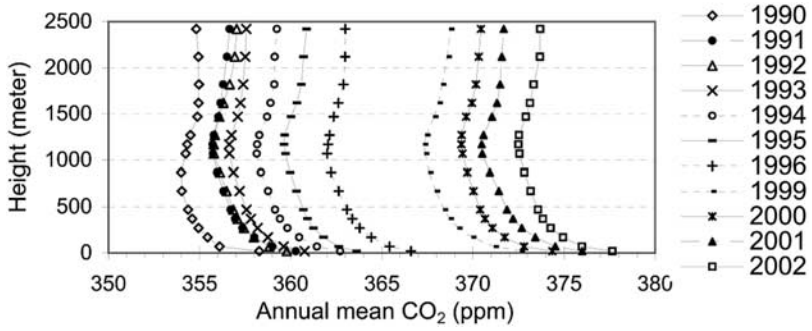

Figure 3. Simulated vertical profiles of the annual mean CO_2 for the period 1990–1996 and 1999–2002, over a boreal region near Fraserdale, Ontario, Canada. The gradients of CO_2 in the atmosphere from the surface layer (e.g., 40 m above the ground) to the annual mean seasonal maximum CBL is a quantitatively measure of the annual total atmospheric rectifier effect.

equal 3.63 ppm, 2.84 ppm and 2.6 ppm for 30 m, 122 m and 396 m, respectively [*Chen et al.*, 2005].

3. Results and Discussion

3.1. Understanding Rectification Mechanism

[18] The net ecosystem CO_2 exchange represents both the diurnal oscillation between photosynthesis and respiration, as well as the seasonal cycle. The atmospheric transport of trace gases has strong diurnal and seasonal components as well because the PBL dynamics varies diurnally and seasonally. The covariation between the terrestrial surface CO_2 flux and the atmospheric transport/convection through dynamics of PBL coherently acts on the same diurnal, synoptic, and seasonal frequencies, which produces vertical and horizontal CO_2 gradients and has been termed as "rectifier" effect [*Keeling et al.*, 1989; *Denning et al.*, 1995]. As discussed in section 2.2, the integrated BEPS-VDS model system has overall capacity of simulating these processes well [*Chen et al.*, 2004]. The model results are useful in understanding the rectification mechanism. The model presentation is divided into the diurnal and seasonal averages in order to differentiate the temporal scales that drive the rectifier effect.

3.1.1. Diurnal Covariance

[19] The monthly composite diurnal covariance during the growing season (e.g., June 2002) is shown in Figure 1, along with the simultaneous surface fluxes, PBL depth and CO_2 mixing ratio profile. The CO_2 flux to the atmosphere (equal to NEE in quantity) simulated by BEPS (Figure 1a) is relatively constant at night with a slight decline from sunset to just prior to sunrise (approximately 3 μmol m^{-2} s^{-1}), which then becomes negative near sunrise and then quickly reaches the minimum value of about -8 μmol m^{-2} s^{-1} by the midmorning (typically around 0930 local time). The photosynthetic uptake decreases slowly during the afternoon and ceases at sunset. The NEE becomes positive again after sunset. The depth of the PBL (Z_i) follows a similar pattern with a shallow (less than 250–300 m), stable NBL (weak mixing) during the night and then with a deep CBL (strong mixing) during daytime. The turbulent CBL begin to develop after sunrise, followed by rapid growth during mid to late morning and reaching a maximum of around 1.25–1.45 km by mid afternoon (Figure 1a). The CO_2 concentration increases due to respiration near the surface in the shallow NBL during the night, and reaches a maximum at sunrise. Soon after sunrise, the CO_2 mixing ratio decreases rapidly due to the entrainment of lower-CO_2 aloft, photosynthetic uptake and turbulent mixing in CBL. Possibly advection could also play a role as well but this is likely minor relative to the other contributing factors [*Yi et al.*, 2000]. The CO_2 mixing ratios reach a minimum during the late afternoon. As a result of this diurnal covariation, the monthly mean CO_2 decreases with height from the ground to the top of CBL (Figure 1c).

3.1.2. Seasonal Covariance

[20] Seasonal covariance between ecosystem metabolism and atmospheric transport occurs in extratropical regions. It plays a crucial role in rectification because seasonal variations are coherent and persistent across latitudinal zones [*Denning et al.*, 1996b; *Yi et al.*, 2004]. The seasonal rectification mechanism is schematic shown in Figure 2

Table 2. Statistics Showing the Observed Annual and Seasonal Mean Air Temperatures and Cumulative Precipitation and Simulated Annual Mean Maximum of Convective Boundary Layer (CBL) Depth and the Annual/Seasonal/Diurnal Atmospheric Rectification of CO_2 for the Periods 1990–1996 and 1999–2002, Fraserdale, Ontario, Canada

Items	1990	1991	1992	1993	1994	1995	1996	1999	2000	2001	2002
Annual mean temperature, °C	1.04	1.23	−0.08	0.4	0.88	0.58	0.76	3.01	1.79	3.44	1.42
Temperature, °C, in Jan	−16.1	−21.4	−17.5	−16.5	−26.5	−15.1	−20.5	−18.7	−18.0	−13.8	−15.7
Temperature °C, in July	17.5	17.3	14.2	17.5	15.9	16.7	15.5	18.7	15.9	16.9	18.7
Annual sum precipitation, mm	930	927	910	766	809	848	784	914	783	897	820
Annual mean CBL, m	995	987	1000	983	981	989	969	1000	980	997	998
Annual rectifier, ppm	4.33	4.57	4.02	4.14	4.58	3.99	4.60	5.32	4.99	5.52	5.15
Diurnal rectifier, ppm	1.25	1.16	0.93	1.08	1.12	0.99	1.05	1.36	1.35	1.31	1.21
Diurnal/annual, %	28.9	25.4	23.2	26.0	24.6	25.0	22.8	25.6	26.9	23.8	23.4

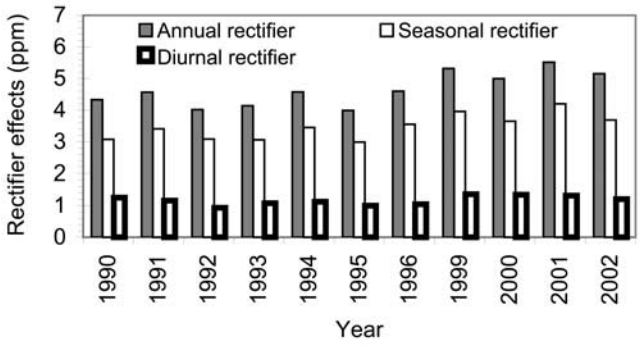

Figure 4. Simulated annual, seasonal and diurnal rectifier effects for the period 1990–1996, 1999–2002, Fraserdale, Ontario, Canada.

through an example from tower observations and simulations for 2002, over the FRD tower area. To examine the seasonal covariance, we focus on the maximum daily CBL depth (Z_{max}, generally occurs from 1230 to 1630 LT), daily integrated surface flux of CO_2 (daily NEE), and the daytime net CO_2 flux to the atmosphere (DNF). The simulated monthly averages of Z_{max}, NEE and DNF are shown in Figure 2a. The CBL depth is much lower during the dormant period of October through March than during in the growing season and also the shallowest in mid-winter. The seasonal variation patterns of NEE and DNF are similar but opposite in phase with CBL depth (Figure 2a). The seasonal covariance is characterized by deeper mixing and larger photosynthetic uptake (downward) during the growing season and by shallower mixing and larger respiration release (upward) during the remaining period of the year. The photosynthesis uptake is diluted through deep mixing in summer, while the respiration release is trapped near the surface in fall and winter. This process produces the annual mean vertical distribution with higher CO_2 mixing ratios at the surface and lower mixing ratios aloft over land (Figure 2c). In other words, the simulated annual mean vertical gradient of CO_2 would reflect the strength of the covariation between vertical transport and the surface flux.

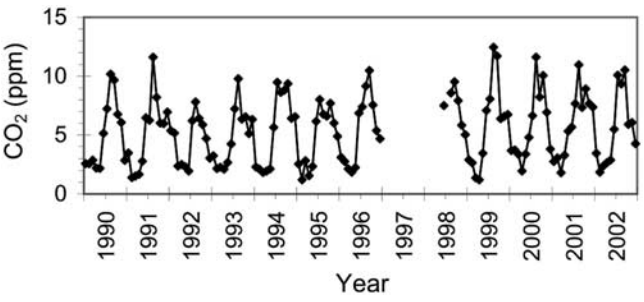

Figure 5. Simulated monthly mean vertical gradients (the difference in CO_2 concentration between the surface layer and the top of CBL), as an indicator of the diurnal rectifier effect) for the periods from February 1990 to the end of 1996 and from June 1998 to the end of 2002, Fraserdale, Ontario, Canada. The diurnal rectifier is found to be much stronger during the growing season than during the dormant season.

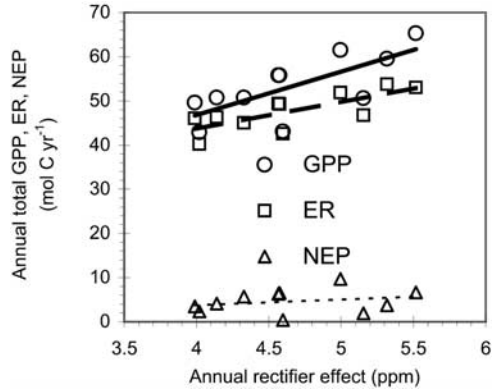

Figure 6. Relationships between the annual rectifier effect (Rec) and annual total GPP, ER, NEP for these 11 years (1990–1996, 1999–2002), Fraserdale, Ontario, Canada. The r^2 for GPP, ER, and NEP were 0.528, 0.571, and 0.065, respectively.

3.2. Interannual Variability in the Rectifier Effect

[21] As shown in Figure 3, the patterns in simulated vertical profiles of annual mean CO_2 for each of the 11 years are similar. The CO_2 mixing ratio decreases with height below the annual mean seasonal maximum CBL height but increases with height above that level. The minimum of the simulated CO_2 mixing ratios through the entire vertical profile occurs around the annual mean seasonal maximum CBL. At the top of model domain, the simulated CO_2 mixing ratios tend to be close to the background value of the FT. However, the gradients of CO_2 in the atmosphere from the surface layer (e.g., 40 m above the ground) to the annual mean seasonal maximum CBL (around 1.2–1.4 km above the ground), as quantitatively measure of the annual total atmospheric rectifier effect, vary from year to year and from location to location as well [*Chen et al.*, 2004; *Denning et al.*, 1996b]. When we performed a model experiment, in which the CO_2 flux derived by BEPS is prescribed without a diurnal cycle (e.g., using daily or monthly mean values), the diurnal

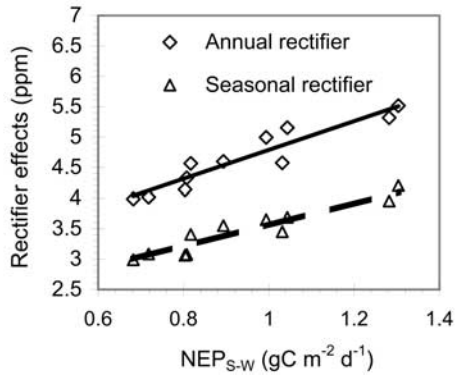

Figure 7. Seasonal amplitude of total daily NEP is highly correlated to seasonal and annual total rectifications (r^2 = 0.894 and 0.8866, respectively) for these 11 years (1990–1996, 1999–2002), Fraserdale, Ontario, Canada. The NEP_{s-w} presents the difference in the seasonal mean total daily NEP between summer and winter.

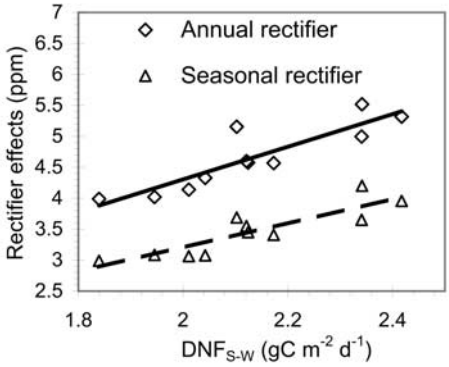

Figure 8. Seasonal amplitude of daytime net flux of CO_2 (DNF) is highly correlated with seasonal and annual total rectifications (r^2 = 0.7741 and 0.784, respectively) for these 11 years (1990–1996, 1999–2002), Fraserdale, Ontario, Canada. The DNF_{s-w} presents the difference in the seasonally averaged DNF between summer and winter.

and seasonal rectifier effects are roughly separated (Table 2 and Figure 4). The simulated gradients of CO_2 from the surface layer to the height of annual mean seasonal maximum CBL using daily or monthly mean fluxes could be the quantity of seasonal rectifying effect (negligible difference are found between using daily and monthly mean values [*Chen et al.*, 2004]). While the difference in the vertical CO_2 profile between those simulated by hourly fluxes and by daily or monthly mean fluxes might come from rectifier effects on other timescales (e.g., diurnal, synoptic). The synoptic effect is expected to be overall much weaker than the diurnal effect. Moreover, the synoptic process can be not directly captured by a 1-D model (i.e., VDS). Therefore, the differences are approximately taken as the diurnal rectifying effect in this study. The diurnal effect accounts for a small part of the difference in the annual mean vertical structure (annual total rectifier effect) [*Denning et al.*, 1996b; *Chen et al.*, 2004]. As listed in Table 2, the annual rectifier effect varies from year to year, ranging from about 3.99 ppm to 5.52 ppm, whereas the diurnal rectification strength ranges from 0.93 ppm to 1.36 ppm. The percentage of diurnal to the total rectification varies in the range from 22.8% to 28.9%. Noticeably, both the seasonal and diurnal components vary from year to year by about ±10% to ±15% of their respective means; that is, the diurnal rectifier has about the same proportion of interannual variability as the seasonal rectifier, but in absolute terms it is a smaller effect. The monthly mean vertical gradient can be considered as an indicator of diurnal rectification strength [*Chen et al.*, 2004], which varies dramatically from season to season and from year to year (Figure 5). Diurnal rectification is found to occur mostly during the growing season.

3.3. Relationship Between Interannual Variability in Rectifier Effect and the Surface CO_2 Fluxes

[22] The influence of terrestrial CO_2 exchange on the distribution of CO_2 in the atmosphere is modulated by the dynamics of the PBL. The strength of the covariance between terrestrial ecosystem metabolism and vertical atmospheric transport/mixing (mainly caused by dynamics of PBL) determines the magnitude of the rectification. The modeled annual mean daily maximum CBL height varies in a narrow range from 970 m to 1000 m during this 11-year period (Table 2), and the variation is not correlated with the rectifier effect. The model results show that the annual total gross primary productivity (GPP) and ecosystem respiration (ER) explain 53% and 57% of the interannual variation in the rectifier effect, respectively, though there is almost no correlation between the interannual variation in the rectifier effect and the net ecosystem productivity (NEP) ($r^2 < 0.07$; Figure 6). However, the difference in NEP between summer and winter is highly correlated with the annual and seasonal rectifications (r^2 = 0.89; Figure 7). Similarly, there is a close relationship between the seasonal amplitude of DNF and the

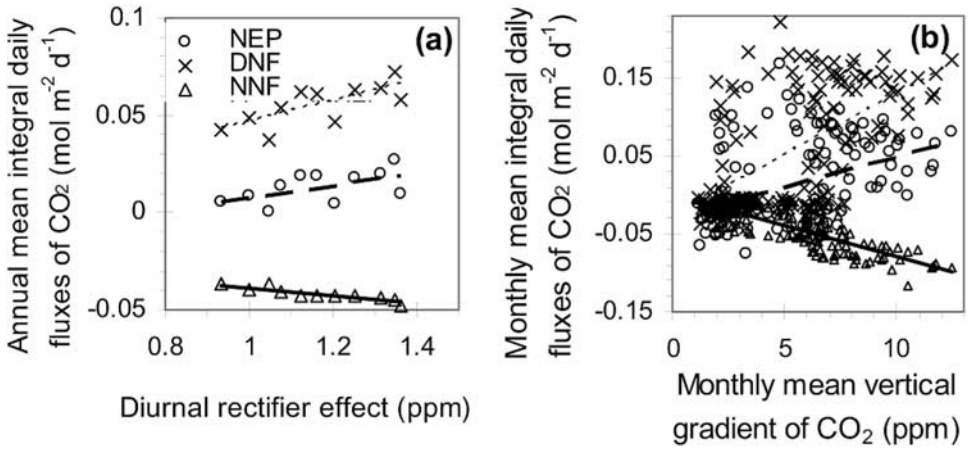

Figure 9. Relationship between the diurnal rectifier effect and daily total surface fluxes of CO_2, Fraserdale, Ontario, Canada. The (a) annual and (b) monthly timescales are given for comparison. The daily total NEP is found to be poorly correlated to diurnal rectification in both monthly and annual timescales, but NNF can explain most of the diurnal rectifier effect. The linear trends are also shown. Solid line, thick dashed line, and thin dashed line are for NNF, NEP, and DNF, respectively, and their r^2 in the same sequence are 0.6659, 0.3494, and 0.1585 for monthly values and 0.8158, 0.5408, and 0.3077 for annual values, respectively.

seasonal rectifications as well (Figure 8). The simulated results also show that both the seasonal amplitudes of NEP and DNF are poorly correlated with the diurnal rectification ($r^2 < 0.5$; $n = 11$). These results are consistent with a simulated result by *Denning et al.* [1996b] in that the covariance between annually balanced terrestrial CO_2 flux and transport in the model still produced a north-south gradient of about 2.5 ppm at the locations of remote marine boundary layer flask stations.

[23] The diurnal rectifier effect is produced by the covariation between the evolution of the diurnal PBL and the surface flux of CO_2. As mentioned above, the monthly mean vertical gradient can be an indicator of diurnal rectification strength, and the annual averaged diurnal rectifier effect could be derived by model experiments. Both of them are plotted with monthly and annual averaged surface fluxes in Figure 9, respectively, to explore surface flux's contributions to the diurnal rectification on various timescales. The daily integral of NEP is found to be poorly correlated with the diurnal rectification at both the monthly and annual timescales, with lower coefficients ($r^2 = 0.35$, 0.54, respectively). However, the regression analysis shows that NNF could explain most of the diurnal rectifier effect. The diurnal rectifier effect is predominantly caused by NNF rather than DNF (r^2: 0.67 versus 0.16 and 0.82 versus 0.31 at monthly and annual temporal scales, respectively). This may be possibly due to the differences between daytime and nighttime in the PBL depth (NBL is normally much shallower than CBL), turbulent mixing strength (much stronger during daytime), and in the entrainment and subsidence (only occurs at daytime).

3.4. Relationship Between Interannual Variability in Rectifier Effect and Climatic Factors

[24] The annual averaged temperatures varies from −0.07° to 3.44°C; while the annual total precipitation varies within a narrow range of 766 to 930 mm per year during the study period (1990–1996 and 1999–2002) (Table 2). Air temperature and moisture are the dominant climatic factors controlling the year-to-year variations in the atmospheric rectifier effect in this particular boreal environment. As shown in Figure 10, the annual rectifier effect is highly correlated with annual mean temperature ($r^2 = 0.84$), while the annual mean air relative humidity explained 51% of the interannual variation in annual rectification (Figure 11). The interannual variation in rectification has poor relationship with annual total precipitation and the growing season length (with $r^2 = 0.005$ and 0.182, respectively) as well.

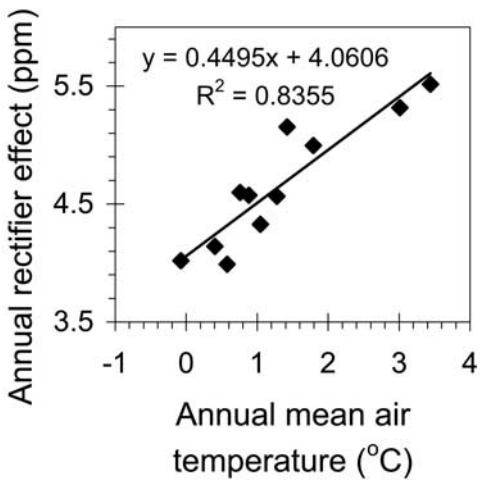

Figure 10. Relationship between the annual rectifier effect and annual mean air temperature for these 11 years (1990–1996, 1999–2002), Fraserdale, Ontario, Canada.

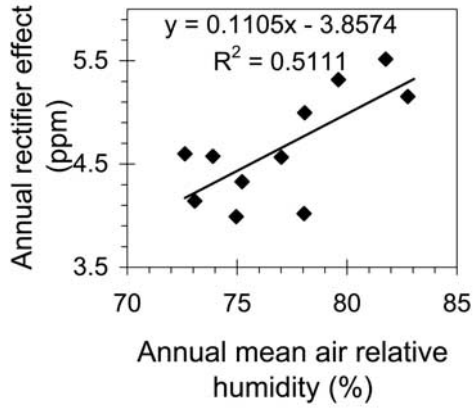

Figure 11. Relationship between the annual rectifier effect and annual mean air relative humidity (RH) for the period 1990–1996, 1999–2002, Fraserdale, Ontario, Canada.

4. Concluding Remarks

[25] The coupled model performs well in simulating CO_2 vertical diffusion processes. The simulated annual atmospheric rectifier effects (including seasonal and diurnal), quantified as the gradient in the mean CO_2 concentration from the surface to the top of PBL, varies from 3.99 to 5.52 ppm, even though the modeled seasonal variations in PBL depth are similar throughout the 11-year period. The inter-annual variations in the rectifier effect primarily result from seasonal changes in the biospheric CO_2 uptake and heterotrophic respiration. The annual mean net ecosystem productivity (NEP) is poorly correlated to the rectifier effect. However, the annual amplitude of NEP (the difference between summer and winter) is highly correlated with annual and seasonal rectifications. NNF explains most of the diurnal rectification (82%) but DNF explains only a small part (31%), reflecting the differences between daytime and nighttime in the PBL depth, the turbulent mixing strength, and the entrainment and subsidence. These results further demonstrate that the atmospheric rectification is not simply influenced by the magnitude of the terrestrial net CO_2 exchange (not a simple function of local source/sink strength), but by seasonal/diurnal variations in the land CO_2 flux and its interaction with PBL dynamics. The covariation between the net CO_2 exchange at the surface and the PBL dynamics depends on daytime, nighttime, seasonal and annual fluxes of CO_2, and this covariation in term affects the spatial distribution of the CO_2 mixing ratio. Understanding the relationship between the vertical gradient in the CO_2 mixing ratio and the surface fluxes is helpful to infer the regional carbon source/sink information using observations at individual towers such as the Fraserdale tower.

[26] Air temperature and moisture are the dominant climatic factors controlling the rectifier effect. The annual rectifier effect was highly correlated with annual mean temperature because both ecosystem respiration and photosynthesis were sensitive to air temperature; while annual mean air relative humidity explained 51% of the annual rectifier effect.

Appendix A: Estimating Solar Irradiance From Air Temperature and Precipitation Data

[27] The daily total solar irradiance at the earth's surface (R_s, $MJm^{-2}s^{-1}$) is estimated by reducing the daily total solar radiation incident at the top of the atmosphere (Q_o, MJ m^{-2} s^{-1}) by the fraction lost due to clouds so that,

$$R_s = \tau Q_o, \tag{A1}$$

where τ is the daily total atmospheric transmittance to solar radiation. τ is devised by *Bristow and Campbell* [1984] as a function of diurnal range of air temperature ($\Delta T = T_{\max} - T_{\min}$, °C),

$$\tau = A\left[1 - \exp\left(-B\Delta T^C\right)\right], \tag{A2}$$

where A, B and C are empirical coefficients unique to specific location. The simplicity of the Bristow-Campbell equation and its predictive accuracy make it attractive. However, it was designed for use on a site-by-site basis with coefficients A, B, and C derived from long-term climatological data [*Bristow and Campbell*, 1984], a procedure that is impractical for analyses over large areas [*Winslow et al.*, 2001]. *Winslow et al* [2001] modified equation (A2) for estimation of R_s with inputs of daily maximum and minimum air temperature, daily total precipitation, mean annual temperature, mean annual temperature range, site latitude, and site elevation. Bristow-Campbell coefficients can be deduced by the following equations after *Winslow et al.* [2001],

$$A = \tau_{cf} D, \tag{A3a}$$

$$B = -\frac{\ln[e_s(T_{\min})/e_s(T_{\max})]}{\Delta T}, \tag{A3b}$$

$$C = -\ln(\Delta T)\left[\ln\left\{\Delta T - \frac{\ln\beta}{B}\right\}\right], \tag{A3c}$$

where τ_{cf} is the atmospheric transmittance of the cloud-free atmosphere; D represent the ratio $R_s/R^{T_{\max}}$ (that is $D = [1 - (H - \pi/4)^2/2H^2]^{-1}$, where H is the half-day length); $e_s(T_{\min})$ and $e_s(T_{\max})$ are saturation vapor pressures at $T_{\min}$ and $T_{\max}$, respectively; and β is an additional parameter required for variation among sites. τ_{cf} is divided into three parts,

$$\tau_{cf} = (\tau_o \tau_a \tau_v)^{P/P_o}, \tag{A4}$$

where τ_o is the transmittance of clean, dry air (= 0.947 − $(1.033 \times 10^{-5})(|\Phi|^{2.22}$ for $|\Phi| \le 80°$ and = 0.774 for $|\Phi| > 80°$, where $|\Phi|$ is the absolute value of the site latitude); τ_a represents the transmittance affected by atmospheric aerosols and ozone, τ_v is the transmittance affected by atmospheric water vapor (= $0.9636 - 9.092 \times 10^{-5}$ $(T_{mean} + 30)^{1.8232}$, where T_{mean} is the annual mean temperature in °C); and P/Po is a correction for site elevation (P is the atmospheric pressure, and P_o is the standard pressure, both in kPa). Following *Winslow et al.* [2001], β is estimated,

$$\beta = \max\{1.041, 23.753\Delta T_m/(T_{mean} + 273.13\}, \tag{A5}$$

where ΔT_m is the mean annual temperature range between $T_{\max}$ and $T_{\min}$.

[28] Once the daily total solar irradiance (R_s) is calculated, its hourly value can be interpolated according to the cosine of solar zenith angle. The model simulations are calibrated and validated against the measured data during 1999–2002 at the FRD site. The squared linear regression coefficient r^2 equals 0.79 and the root mean square error (RMSE) equals 41 Wm^{-2}.

[29] **Acknowledgments.** This work is supported by the Canadian Foundation for Climate and Atmospheric Sciences (project GC423). We thank Peter Bakwin and Pieter Tans of the NOAA/CMDL Carbon Cycle Group, who provided reference MBL matrix data of CO_2 mixing ratio. We would like to acknowledge Jane Liu (Department of Physics, University of Toronto, Canada), and Kaz Higuchi, Douglas Chan and Lin Huang of Meteorological Service of Canada for useful discussions on early part of our results. We are grateful to Steven C. Wofsy and Ian G. Enting for their constructive reviews and suggestions that improved the manuscript.

References

Arain, M. A., T. A. Black, A. G. Barr, P. G. Jarvis, J. M. Massheder, D. L. Verseghy, and Z. Nesic (2002), Effects of seasonal and interannual climate variability on net ecosystem productivity of boreal deciduous and conifer forests, *Can. J. For. Res.*, *32*(5), 878–891.

Bakwin, P., P. P. Tans, C. Zhao, W. Ussler, and E. Quesnell (1995), Measurements of carbon dioxide on a very tall tower, *Tellus, Ser. B*, *47*, 535–549.

Bakwin, P. S., P. P. Tans, D. F. Hurst, and C. Zhao (1998a), Measurements of carbon dioxide on very tall towers: Results of the NOAA/CMDL program, *Tellus, Ser. B*, *50*, 401–415.

Bakwin, P., P. P. Tans, J. W. C. White, and R. J. Andres (1998b), Determination of the isotopic ($^{13}C/^{12}C$) discrimination by terrestrial biology from a global network of observations, *Global Biogeochem. Cycles*, *12*, 555–562.

Blasing, T. J., C. T. Bronlank, and G. Marland (2005), The annual cycle of fossil-fuel carbon dioxide emissions in the United States, *Tellus, Ser. B*, *57*, 107–115.

Bolin, B., and C. D. Keeling (1963), Large-scale atmospheric mixing as deduced from the seasonal and meridional variations of carbon dioxide, *J. Geophys. Res.*, *68*(13), 3899–3920.

Bristow, K. L., and G. S. Campbell (1984), On the relationship between incoming solar radiation and daily maximum and minimum temperature, *Agric. For. Meteorol.*, *31*, 159–166.

Chen, B., J. M. Chen, J. Liu, D. Chan, K. Higuchi, and A. Shashkov (2004), A Vertical Diffusion Scheme to estimate the atmospheric rectifier effect, *J. Geophys. Res.*, *109*, D04306, doi:10.1029/2003JD003925.

Chen, J. M., J. Liu, J. Cihlar, and M. L. Goulden (1999), Daily canopy photosynthesis model through temporal and spatial scaling for remote sensing applications, *Ecol. Modell.*, *124*, 99–119.

Chen, J. M., B. Chen, P. Tans, and K. J. Davis (2005), Deriving photosynthetic and respiratory fluxes from CO_2 mixing ratios measured on the Wisconsin tall tower, *Eos Trans. AGU*, *85*(17), Jt. Assem. Suppl., Abstract 99.

Chou, W. W., S. C. Wofsy, R. C. Harriss, J. C. Lin, C. Gerbig, and G. W. Sachse (2002), Net fluxes of CO_2 in Amazonia derived from aircraft observations, *J. Geophys. Res.*, *107*(D22), 4614, doi:10.1029/2001JD001295.

Conway, T. J., et al. (1994), Evidence for interannual variability of the carbon cycle from the NOAA/CMDL global air sampling network, *J. Geophys. Res.*, *99*(D11), 22,831–22,855.

Denning, A. S., I. Y. Fung, and D. A. Randall (1995), Latitudinal gradient of atmospheric CO_2 due to seasonal exchange with land biota, *Nature*, *376*, 240–243.

Denning, A. S., G. J. Collatz, C. Zhang, D. A. Randall, J. A. Berry, P. J. Sellers, G. D. Colello, and D. A. Dazlich (1996a), Simulations of terrestrial carbon metabolism and atmospheric CO_2 in a general circulation model: Part 1, Surface carbon fluxes, *Tellus, Ser. B*, *48*, 521–542.

Denning, A. S., D. A. Randall, G. J. Collatz, and P. J. Sellers (1996b), Simulations of terrestrial carbon metabolism and atmospheric CO_2 in a general circulation model: Part 2: Simulated CO_2 concentrations, *Tellus, Ser. B*, *48*, 543–567.

Denning, A. S., T. Takahashi, and P. Friedlingstein (1999), Can a strong atmospheric CO_2 rectifier effect be reconciled with a "reasonable" carbon budget?, *Tellus, Ser. B*, *51*, 250–253.

Enting, I. G. (1999), Characterising the temporal validity of the global carbon cycle, *Tech. Pap. 40*, CSIRO Atmos. Res., Hobart, Tasmania, Australia.

Enting, I. G., C. M. Trudinger, and R. J. Francey (1995), A synthesis inversion of the concentration and $\delta^{13}C$ of atmospheric CO_2, *Tellus, Ser. B*, *47*, 35–52.

Farquhar, G. D., S. Caemmerer, and S. Berry (1980), A biochemical model of photosynthetic CO_2 assimilation in leaves of C_3 species, *Planta*, *149*, 78–90.

Francey, R., C. E. Allison, I. G. Enting, J. W. C. White, M. Trolier, and P. P. Tans (1995), Changes in the oceanic and terrestrial carbon uptake since 1982, *Nature*, *373*, 326–330.

Fung, I. Y., C. J. Tucker, and K. C. Prentice (1987), Application of advanced very high-resolution radiometer vegetation index to study atmosphere-biosphere exchange of CO_2, *J. Geophys. Res.*, *92*(D3), 2999–3015.

GLOBALVIEW-CO2 (2004), *Cooperative Atmospheric Data Integration Project—Carbon Dioxide* [CD-ROM], NOAA Clim. Monit. and Diag. Lab., Boulder, Colo. (Available via anonymous FTP to ftp.cmdl.noaa.gov, Path: ccg/co2/GLOBALVIEW)

Gloor, M., S.-M. Fan, S. Pacala, and J. Sarmiento (2000), Optimal sampling of the atmosphere for purpose of inverse modeling: A model study, *Global Biogeochem. Cycles*, *14*, 407–428.

Gurney, R. K., et al. (2002), Towards robust regional estimates of CO_2 sources and sinks using atmospheric transport models, *Nature*, *415*, 626–630.

Gurney, K. R., et al. (2003), TransCom3 CO_2 inversion intercomparison: 1. Annual mean control results and sensitivity to transport and prior flux information, *Tellus, Ser. B*, *55*, 555–579.

Higuchi, K., et al. (2003), Regional source/sink impact on the diurnal, seasonal and inter-annual variations in atmospheric CO_2 at a boreal forest site in Canada, *Tellus, Ser. B*, *55*, 115–125.

Ishizawa, M., T. Nakazawa, and K. Higuchi (2002), A multi-box model study of the role of the biospheric metabolism in the recent decline of $\Delta^{18}O$ in the atmospheric CO_2, *Tellus, Ser. B*, *54*, 307–324.

Ju, W., J. M. Chen, and B. Chen (2004), Modelling the response of energy, water, and CO_2 fluxes over forest to climate variability, AGU 2004 Spring Meeting, *Eos Trans. AGU*, *85*(17), Jt. Assem. Suppl., Abstract B13A-01.

Keeling, C. D., R. B. Bacastow, A. E. Bainbridge, C. A. Ekdahl, P. R. Guenther, L. S. Waterman, and J. F. S. Chin (1976), Atmospheric carbon dioxide variations at Mauna Loa observatory, Hawaii, *Tellus, Ser. B*, *28*, 538–551.

Keeling, C. D., R. B. Bacastow, A. F. Carter, S. C. Piper, T. P. Whorf, M. Heimann, W. G. Mook, and H. Roeloffzen (1989), A three-dimensional model of atmospheric CO_2 transport based on observed winds: 1. Analysis of observed data, in *Aspects of Climate Variability in the Pacific and Western Americas*, *Geophys. Monogr. Ser.*, vol. 55, edited by D. H. Peterson, pp. 165–236, AGU, Washington, D. C.

Keeling, C. D., T. P. Whorf, M. Whalen, and J. van der Plicht (1995), Interannual extremes in the rate of rise of atmospheric carbon dioxide since 1980, *Nature*, *375*, 666–670.

Lacelle, B. (1998), Canada's soil organic carbon database, in *Soil Processes and the Carbon Cycle*, edited by R. Lal et al., pp. 93–101, CRC Press, Boca Raton, Fla.

Law, R. M., et al. (1996), Variations in modeled atmospheric transport of carbon dioxide and the consequence for CO_2 inversions, *Global Biogeochem. Cycles*, *10*, 783–796.

Liu, J., J. M. Chen, J. Cihlar, and W. M. Park (1997), A process-based boreal ecosystem productivity simulator using remote sensing inputs, *Remote Sens. Environ.*, *62*, 158–175.

Liu, J., J. M. Chen, J. Cihlar, and W. Chen (1999), Net primary productivity distribution in BOREAS region from a process model using satellite and surface data, *J. Geophys. Res.*, *104*(D22), 27,735–27,754.

Liu, J., J. M. Chen, J. Cihlar, and W. Chen (2002), Net primary productivity mapped for Canada at 1-km resolution, *Global Ecol. Biogeogr.*, *11*, 115–129.

Marland, G., T. A. Boden, and R. J. Andres (2002), Global, regional, and national CO_2 emissions, in *Trends: A Compendium of Data on Global Change*, Carbon Dioxide Inf. Anal. Cent., Oak Ridge, Tenn.

Matsushita, B., and M. Tamura (2002), Integrating remotely sensed data with an ecosystem model to estimate net primary productivity in East Asia, *Remote Sens. Environ.*, *81*, 58–66.

Matsushita, B., M. Xu, J. Chen, S. Kameyamad, and M. Tamura (2004), Estimation of regional net primary productivity (NPP) using a process-based ecosystem model: How important is the accuracy of climate data?, *Ecol. Modell.*, *178*, 371–388.

McNaughton, K. G., and T. W. Spriggs (1986), A mixed-layer model for regional evaporation, *Boundary Layer Meteorol.*, *34*, 231–246.

Olsen, S. C., and J. T. Randerson (2004), Differences between surface and column atmospheric CO_2 and implications for carbon cycle research, *J. Geophys. Res.*, *109*, D02301, doi:10.1029/2003JD003968.

Prentice, I. C., et al. (2001), The scientific basis, in *Climate Change 2001*, edited by J. T. Houghton and D. Yihui, chap. 3, pp. 183–237, Cambridge Univ. Press, New York.

Rayner, P. J., and D. M. O'Brien (2001), The utility of remotely sensed CO_2 concentration data in surface source inversions, *Geophys. Res. Lett.*, *28*(1), 175–178.

Rayner, P. J., R. M. Law, D. M. O'Brien, T. M. Butler, and A. C. Dilley (2002), Global observations of the carbon budget: 3. Initial assessment of the impact of satellite orbit, scan geometry, and cloud on measuring CO_2 from space, *J. Geophys. Res.*, *107*(D21), 4557, doi:10.1029/2001JD000618.

Schut, P., J. Shields, C. Tarnocai, D. Coote, and I. Marshall (1994), Soil landscapes of Canada—An environmental reporting tool, paper presented at Canadian Conference on GIS Proceedings, Can. Inst. of Surv. and Mapping, Ottawa.

Sellers, P. J., et al. (1996), A revised land surface parameterization (SiB2) for atmospheric GCMs: Part 1. Model formulation, *J. Clim.*, *9*, 676–705.

Sellers, P. J., et al. (1997), Modeling the exchange of energy, water, and carbon between continentals and the atmosphere, *Science*, *275*, 502–509.

Shields, J. A., C. Tarnocai, K. W. G. Valentine, and K. B. MacDonald (1991), Soil landscapes of Canada, procedures manual and user's hand book, *Publ. 1868/E*, Agric. Can., Ottawa.

Stephens, B. B., S. C. Wofsy, R. F. Keeling, P. P. Tans, and M. J. Potosnak (2000), The CO_2 budget and rectification airborne study: Strategies for measuring rectifiers and regional fluxes, *Geophys. Monogr.*, *14*, 311–324.

Stull, R. B. (1993), *An Introduction to Boundary Layer Meteorology*, Springer, New York.

Sun, R., J. M. Chen, Y. Zhou, Q. Zhu, J. Liu, J. Li, S. Liu, G. Yan, and S. Tang (2004), Estimation of net primary productivity and evapotranspiration in Changbaishan, China using ETM data, *Can. J. Remote Sens.*, *30*(5), 731–742.

Tans, P. P., I. Y. Fung, and T. Takahashi (1990), Observational constraints on the global atmospheric CO_2 budget, *Science*, *247*, 1431–1438.

Tans, P. P., P. S. Bakwin, and D. W. Guenther (1996), A feasible global carbon cycle observing system: A plan to decipher today's carbon cycle based on observations, *Global Change Biol.*, *2*, 309–318.

Tarnocai, C. (1996), The amount of organic carbon in various soil orders and ecological provinces in Canada, in *Soil Processes and the Carbon Cycle*, edited R. Lal et al., pp. 81–92, CRC Press, Boca Raton, Fla.

Wang, Q., J. Tenhunen, E. Falge, C. H. Bernhofer, A. Granier, and T. Vesala (2003), Simulation and scaling of temporal variation in gross primary production for coniferous and deciduous temperate forests, *Global Change Biol.*, *10*, 37–51, doi:10.1046/j.1529-8817.2003.00716.x.

Wang, S. S., R. F. Grant, D. L. Verseghy, and T. A. Black (2002a), Modelling carbon-coupled energy and water dynamics of a boreal aspen forest in a general circulation model land surface scheme, *Int. J. Climatol.*, *22*(10), 1249–1265.

Wang, S. S., R. F. Grant, D. L. Verseghy, and T. A. Black (2002b), Modelling carbon dynamics of boreal forest ecosystems using the Canadian Land Surface Scheme, *Clim. Change*, *55*(4), 451–477.

Winslow, J. C., E. R. Hunt Jr., and S. C. Piper (2001), A globally applicable model of daily solar irradiance estimated from air temperature and precipitation data, *Ecol. Modell.*, *143*, 227–243.

Wofsy, S. C., and R. C. Harris (2002), The North American Carbon Program (NACP): Report of the NACP Committee of the U.S. Interagency Carbon Cycle Science Program, report, U.S. Global Change Res. Program, Washington, D. C. (Available at http://www.esig.ucar.edu/nacp/)

Wofsy, S. C., R. C. Harriss, and W. A. Kaplan (1988), Carbon dioxide in the atmosphere over the Amazon basin, *J. Geophys. Res.*, *93*(D2), 1377–1387.

Yi, C. K., et al. (2000), The influence of advection on measurements of the net ecosystem-atmosphere exchange of CO_2 from a very tall tower, *J. Geophys. Res.*, *105*(D8), 9991–9999.

Yi, C. K., et al. (2004), Observed covariance between ecosystem carbon exchange and atmospheric boundary layer dynamics at a site in northern Wisconsin, *J. Geophys. Res.*, *109*, D08302, doi:10.1029/2003JD004164.

Zilitinkevich, S., and A. Baklanov (2002), Calculation of the height of the stable boundary layer in practical applications, *Boundary Layer Meteorol.*, *105*, 389–409.

Zilitinkevich, S., and D. V. Mironov (1996), A multi-limit formulation for the equilibrium depth of a stably stratified boundary layer, *Boundary Layer Meteorol.*, *81*, 325–351.

Zilitinkevich, S., A. Baklanov, J. Rost, A.-S. Smedman, V. Lykosov, and P. Calanca (2002), Diagnostic and prognostic equations for the depth of the stably stratified Ekman boundary layer, *Q. J. R. Meteorol. Soc.*, *128*, 25–46.

B. Chen and J. M. Chen, Department of Geography and Program in Planning, University of Toronto, 100 St. George Street, Room 5047, Toronto, Ontario, Canada M5S 3G3. (chenb@geog.utoronto.ca; chenj@geog. utoronto.ca)

D. E. J. Worthy, Air Quality Research Branch, Meteorological Service of Canada, EC, 4905 Dufferin Street, Toronto, Ontario, Canada M3H 5T4. (doug.worthy@ec.gc.ca)